Journal of Sound and Vibration (1998) **212**(2), 265–274

FINITE ELEMENT MODELLING OF RADIATING WAVES IN IMMERSED WEDGES

A.-C. Hladky-Hennion, P. Langlet and R. Bossut

IEMN (*UMR* 9929 *CNRS*), *departement ISEN*, 41 *Boulevard Vauban*, 59046 *Lille Cedex*, *France*

AND

M. de Billy

Groupe de Physique des Solides, *Université Paris* 7, *Tour* 23, 2 *Place Jussieu*, 75251 *Paris Cedex* 05, *France*

(*Received* 19 *May* 1997, *and in final form* 19 *November* 1997)

The propagation of acoustic waves in immersed waveguides has been previously studied with the help of the finite element method, by using the ATILA code (A. C. Hladky-Hennion *et al*., 1997 JSV **200**, 519–530). In that paper, the study of the propagating modes along immersed rectilinear wedges was presented, and the theoretical results obtained for Plexiglas wedges agreed well with the experiments. Nevertheless, due to the theoretical formulation, the method was not able to study radiating modes. Thus, the present paper presents a modification of the previous method, with a view to finding either propagating modes or radiating modes. First the formalism is presented, where an original procedure is used to solve the finite element system. Then, wedges, the top angle of which varies, are studied and the finite element results for the wedge wave velocity are compared to experiments, for brass and duralumin samples.

1. INTRODUCTION

The propagation of flexural wedge waves along a linear elastic edge in contact with air have attracted interest because these waves are dispersionless, their propagation velocity is lower than the Rayleigh wave velocity and the acoustic energy is confined at the tip of the wedge guide. Thus, they have been extensively investigated theoretically and experimentally [1–8]. More recently, different authors have demonstrated [3, 4, 6, 7] that the water loading effect implies a decrease in the velocity of propagation of the flexural modes. As the boundary conditions of the problem are complex, the use of the finite element method to tackle the problem can strongly broaden the designer's possibilities, particularly because it allows the modelling of any cross-section geometry, by simply building specific meshes, without any new algebraic development.

Initially, Lagasse [1] applied the finite element method to analyze the propagation of the acoustic waves in an infinite waveguide of arbitrary cross-section in air. Lagasse's technique is original because the problem is reduced to a bidimensional problem, where only the cross-section of the guide is meshed by using finite elements. It has been used in the case of curved [5] and immersed waveguides [6]. That was an interesting innovation because, to the authors' knowledge, theoretical or numerical modelling of the immersed solid wedge had not yet been developed in the general case.

0022–460X/98/170265 + 10 $25.00/0/sv971408

But, until now, the method was restricted to the analysis of the propagating waves along the wedge without re-emission in the fluid. Due to the theoretical formulation, the method was not able to study radiating modes. In the case of immersed Plexiglas samples, the method has allowed one to determine that the limit of the wedge wave velocity in water for large apex angles is the Stoneley–Scholte wave velocity [6, 9, 10].

This paper presents an extension of the technique to the analysis of acoustic waves in immersed waveguides, with a view to finding either propagating or radiating modes. First, it presents the theoretical formulation for immersed linear waveguides, where an original procedure is used to solve the finite element system, that has been incorporated in the ATILA finite element code [11]. Then, the wave velocity of the wedge, the top angle of which is variable, is studied and the finite element results are compared to the experiments, for immersed brass and duralumin wedges. The visualization of the waves propagating or radiating in the fluid authorizes a good knowledge of the problem.

2. THEORETICAL FORMULATION

The formalism has been extensively described in references [5] and [6]. Thus, only the main results are reproduced here. An acoustic wave, characterized by its wavenumber k_z, is propagating along a uniform, infinite and immersed waveguide, in the z direction. Because the section of the waveguide is uniform in the z direction, it is possible to solve the problem with the help of a bidimensional mesh and to reconstitute the whole solution [1, 6]. The section of the waveguide is meshed with the help of the finite element method. In the xy-plane (see Figure 1), the whole domain contains a solid domain S_s and a fluid domain S_f separated by the l_i interface line. The fluid domain is limited by the l_r radiating line. On this line, a non-reflecting condition is applied, by considering a pressure field which is essentially monopolar [12]. The whole domain is split into elements connected by nodes.

With a view to finding the eigenmodes and considering the propagating wave in the z direction, the final system of equations, previously described in reference [6], is

$$\begin{bmatrix} [K]-\omega^2[M] & -[L] \\ -\rho_f^2 c_f^2 \omega^2 [L]^{\mathrm{T}} & [H]-\omega^2[M_1]+\dfrac{\rho_f c_f^2}{R}\left[\tfrac{1}{2}-\mathrm{j}k_r R\right][D] \end{bmatrix} \begin{pmatrix} \underset{\sim}{U} \\ \underset{\sim}{P} \end{pmatrix} = \begin{pmatrix} \underset{\sim}{0} \\ \underset{\sim}{0} \end{pmatrix}, \tag{1}$$

where $[K]$ is the stiffness matrix in the solid domain. It is written as

$$[K] = [K_0] + k_z[K_1] + k_z^2[K_2], \tag{2}$$

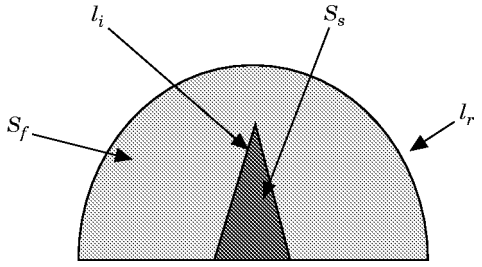

Figure 1. Traces of the finite element domains in the xy plane.

where $[K_0]$, $[K_1]$ and $[K_2]$ are all real symmetric matrices because the material is lossless. The $[K_0]$, $[K_1]$ and $[K_2]$ matrices are independent of k_z. The stiffness matrix is calculated by integrating over the x and y variables on the cross-section S_s. Thus, the displacement field is z dependent but a bidimensional mesh, depending on x and y, is sufficient to take into account the propagating wave in the z direction. $[M]$ is the mass matrix in the solid domain and is k_z independent. $[H]$ is the compressibility matrix in the fluid domain and is written as

$$[H] = [H_0] + k_z^2[H_2], \tag{3}$$

where $[H_0]$ and $[H_2]$ are real symmetric matrices and independent of k_z. The compressibility matrix is calculated by integrating over the x and y variables on the cross section S_f.

$[M_1]$ is the mass matrix in the fluid domain and is k_z independent. $[L]$ is the interface matrix, which represents the coupling between the fluid and the solid on the l_i line and is k_z independent. Because of a non-reflecting condition on the external fluid l_r line, the $[D]$ matrix relating the pressure normal derivative and the pressure on the surface, is introduced in the system but is k_z independent. This non-reflecting condition is valid if the external fluid boundary is outside the near field area ($|k_r R| \gg 1$). k_r is the radial component of the wavevector. In that case, the decreasing of the pressure field is proportional to $e^{jk_r R}/\sqrt{R}$. ρ_f and c_f are respectively the density and the sound speed in the fluid. These two terms are real, because the fluid is assumed to be lossless. R is the radius of the external fluid boundary. k_r is related to k_z by the relation

$$k^2 = k_r^2 + k_z^2 = \omega^2/c_f^2. \tag{4}$$

From now on, all the matrices appearing in the finite element system of equation (1) are written as functions of k_z. In the previous study [6], the given wavenumber k_z was real. Thus, the modal analysis of the system has given ω, the angular frequency and the corresponding eigenvectors: $\underline{U}$, the vector of the nodal values of the displacement field and $\underline{P}$, the vector of the nodal values of the pressure field. But, because the given wavenumber k_z was real, only the propagating modes were identified, without attenuation in the waveguide direction. These modes correspond to a real frequency and an imaginary k_r wavenumber, because the mode is attenuated in the radial direction. This is in agreement with the search for edge waves, the amplitudes of displacement of which are located in the vicinity of the apex of the wedge [2]. Thus, with a view to finding either propagating or radiating modes, the system is modified, keeping a real angular frequency. Upon using the original variable change

$$k_z = [(1 - y^2)/(1 + y^2)]\omega/c_f \qquad \text{and} \qquad k_r = [2y/(1 + y^2)]\omega/c_f, \tag{5}$$

equation (1) becomes

$$([A] + y[B] + y^2[C] + y^3[B] + y^4[E])\underline{X} = \underline{0}, \tag{6}$$

where

$$[A] = \begin{bmatrix} [K_0] + \dfrac{\omega}{c_f}[K_1] + \dfrac{\omega^2}{c_f^2}[K_2] - \omega^2[M] & -[L] \\ -\rho_f^2 c_f^2 \omega^2 [L]^{\mathrm{T}} & [H_0] + \dfrac{\omega^2}{c_f^2}[H_2] - \omega^2[M_1] + \dfrac{\rho_f c_f^2}{2R}[D] \end{bmatrix},$$

$$[B] = 2\begin{bmatrix} [0] & [0] \\ [0] & -j\omega\rho_f c_f [D] \end{bmatrix},$$

TABLE 1

Physical constants of the materials: *density*, *longitudinal wave velocity* (V_l), *transverse wave velocity* (V_t), *Rayleigh wave velocity* (V_R)

Material	Density (kg/m^3)	V_l (m/s)	V_t (m/s)	V_R (m/s)
Brass	8600	4348	2126	1985
Duralumin	2700	6350	3100	2894

$$[C] = 2 \begin{bmatrix} [K_0] - \dfrac{\omega^2}{c_f^2}[K_2] - \omega^2[M] & -[L] \\ -\rho_f^2 c_f^2 \omega^2 [L]^{\mathrm{T}} & [H_0] - \dfrac{\omega^2}{c_f^2}[H_2] - \omega^2[M_1] + \dfrac{\rho_f c_f^2}{2R}[D] \end{bmatrix},$$

$$[E] = \begin{bmatrix} [K_0] - \dfrac{\omega}{c_f}[K_1] + \dfrac{\omega^2}{c_f^2}[K_2] - \omega^2[M] & -[L] \\ -\rho_f^2 c_f^2 \omega^2 [L]^{\mathrm{T}} & [H_0] + \dfrac{\omega^2}{c_f^2}[H_2] - \omega^2[M_1] + \dfrac{\rho_f c_f^2}{2R}[D] \end{bmatrix},$$

$$\underset{\sim}{X} = \begin{pmatrix} \underset{\sim}{U} \\ \underset{\sim}{P} \end{pmatrix}. \tag{7}$$

With a view to solving equation (7), the system is once again modified and is written as

$$\left(\begin{bmatrix} [0] & [0] & [0] & [A] \\ [0] & [0] & [A] & [B] \\ [0] & [A] & [B] & [C] \\ [A] & [B] & [C] & [B] \end{bmatrix} + y \begin{bmatrix} [0] & [0] & [-A] & [0] \\ [0] & [-A] & [-B] & [0] \\ [-A] & [-B] & [-C] & [0] \\ [0] & [0] & [0] & [E] \end{bmatrix} \right) \begin{pmatrix} \underset{\sim}{X} \\ y\underset{\sim}{X} \\ y^2\underset{\sim}{X} \\ y^3\underset{\sim}{X} \end{pmatrix} = \begin{pmatrix} \underset{\sim}{0} \\ \underset{\sim}{0} \\ \underset{\sim}{0} \\ \underset{\sim}{0} \end{pmatrix}. \tag{8}$$

Finally the system size is $4N \times 4N$, where N is the initial number of equations. For a given real angular frequency ω, the $[A]$, $[B]$, $[C]$ and $[E]$ matrices are built and the system is solved, with the help of Lanczos classical iterative algorithms [13–15]. The eigenvalues calculation gives the y values. Then, the k_z and k_r wavenumbers are deduced, by using equation (5). The corresponding eigenvectors give the displacement field and the pressure field in the $z = 0$ plane. It is easy to reconstitute the displacement field and the pressure field in the $z = z_0$ plane by multiplying the eigenvectors by $e^{jk_z z_0}$. Additional modes are obtained due to the far field approximation of the radiating condition [6]. They are easily located with the help of the pressure field in the fluid and on the external fluid boundary. Moreover, these modes are characterized by a pressure which is greater on the external fluid boundary than on the wedge. Thus, their eigenvalues are sufficiently separated from those of the interesting modes; the eigenvectors are truly orthogonal. They are not of interest in this study. Finally, the propagation modes are characterized by their wave velocity, which is the ratio between the eigenangular frequencies and the k_z wavenumber. The calculations are performed for different values of the given real angular frequency and for each case, the wave velocity is deduced. In the case of wedges, it is shown that the wave velocity remains constant, when the mesh criteria are verified.

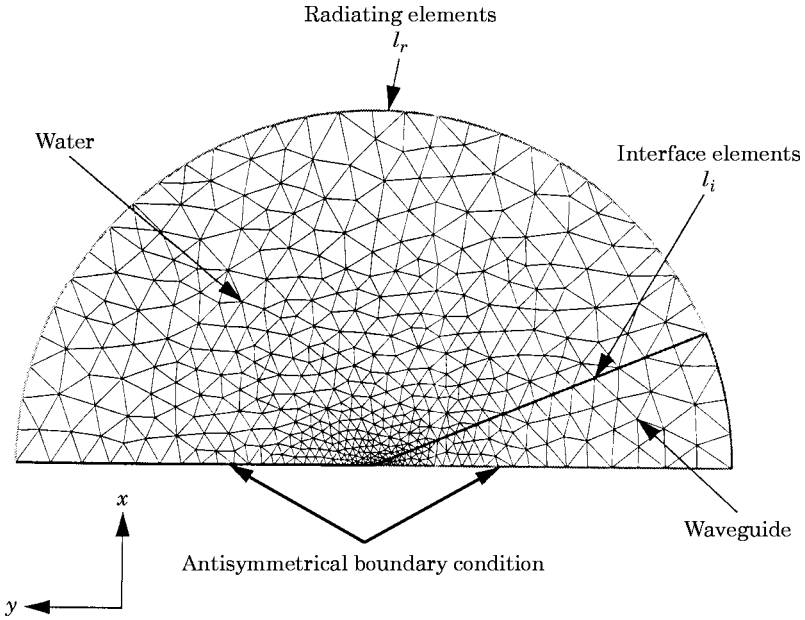

Figure 2. Finite element mesh of the immersed wedge.

3. IMMERSED BRASS WEDGE

In this section, brass wedge samples are considered, with different apex angles, varying by a 5° step. The physical constants of this material used for the calculation are presented in Table 1. The analysis of the wedge in air has already been performed [6] and only the results are reproduced in this paper, for comparison. Here, the brass sample is immersed in water. Figure 2 presents the finite element mesh of the immersed wedge, containing a solid part, a fluid part, the interface line l_i between the fluid and the solid, and the radiating elements on the external fluid line. In all the following examples, isoparametric elements are used, with a quadratic interpolation along the elements sides. Then, the classical $\lambda/4$ criterion has to be verified, which states that the largest length of each element in a given

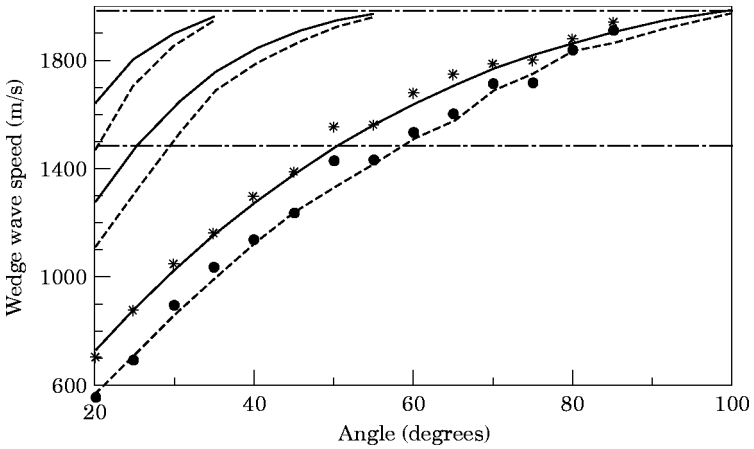

Figure 3. Variations of the wedge wave velocities, as a function of the apex angle for the immersed brass wedge. Full line: finite element results of the in-air wedge; dashed lines: finite element results for the immersed wedge; crosses: experimental results for the in-air wedge; black points: experimental results for the immersed wedge.

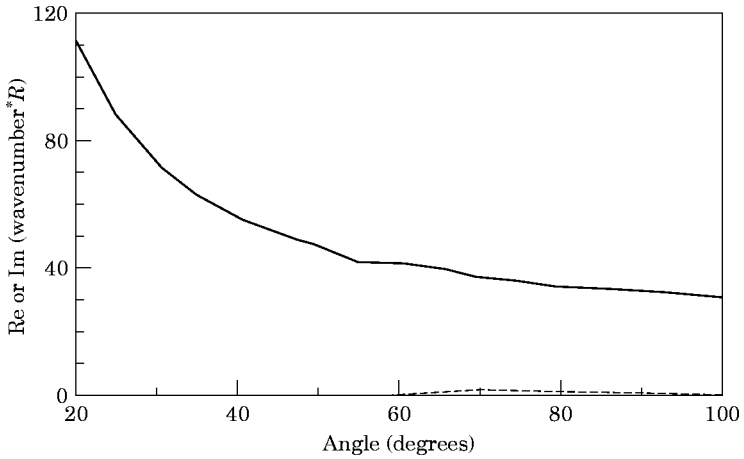

Figure 4. Variations of the k_z wavenumber as a function of the apex angle, for the immersed brass wedge. Full line: Re ($k_z R$); dashed line: Im ($k_z R$).

mesh has to be smaller than a quarter of the wavelength for the working frequency. Upon applying a monopolar condition on the external fluid boundary of the finite element mesh and for a given real angular frequency, the eigenmodes are calculated.

Figure 3 presents the variations of the wedge wave velocities of the immersed brass sample as a function of the apex angle. In the case of small apex angles, several antisymmetrical flexural modes exist [16]. The curves reproduced in Figure 3 also show the variations of the wedge wave velocities of the in-air brass sample [6]. They indicate that the water loading induces a decrease in the wedge wave velocities, which is greater for small apex angles. The agreement is good between the finite element results and the experimental data obtained for the first mode. The acoustic technique applied to the measurement of the wave velocity for immersed wedges is the same as the one used for the measurement of the free edge wave velocity [17]. To verify the influence of the liquid loading effect, the whole set-up was immersed in the fluid [7].

Figure 4 presents the variations of the k_z wavenumber, multiplied by the radius R of the external fluid boundary, as a function of the apex angle. The wavenumber is complex and both its real and imaginary parts are reproduced.

If the wedge wave velocity is subsonic, i.e. if the apex angle is lower than approximately 60° for the first mode and approximately 30° for the second mode, the wave is propagating in the z direction. The k_z wavenumber is real and there is no remission in the fluid.

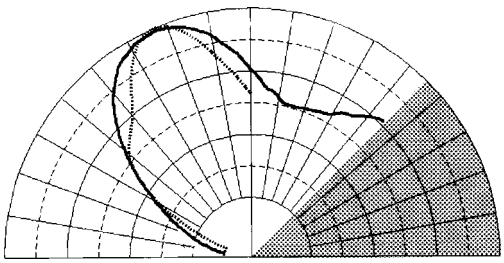

Figure 5. First antisymmetrical wedge mode of a brass sample immersed in water. Half apex angle = 45°; $|k_r R| = 26{\cdot}40$. Normalized pressure field in a plane perpendicular to the wedge direction, with a linear scale. Full line: finite element results; dashed line: experimental results.

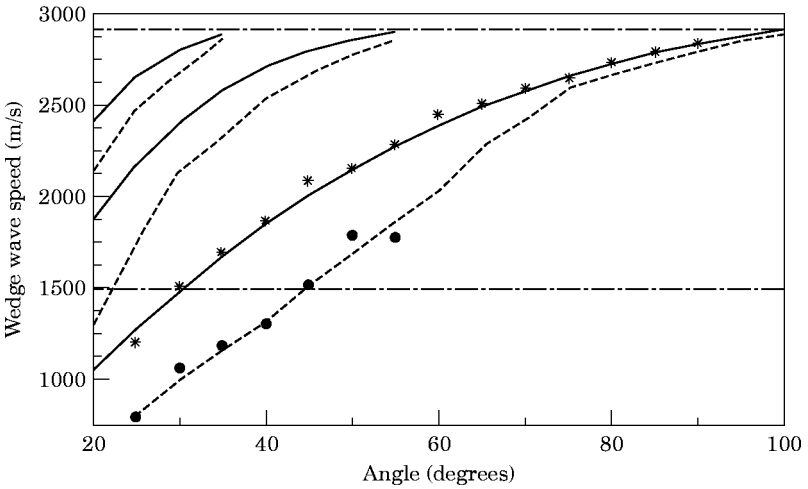

Figure 6. Variations of the wedge wave velocities as a function of the apex angle, for the immersed duralumin wedge. Full line: finite element results for the in-air wedge; dashed lines: finite element results for the immersed wedge; crosses: experimental results for the in-air wedge; black points: experimental results for the immersed wedge.

If the wedge wave velocity is supersonic, i.e., if the apex angle is greater than approximately 60° for the first mode and approximately 30° for the second mode, k_z wavenumber is complex. The wave propagates and is attenuated in the z direction, which means that this propagating mode radiates energy in the fluid. For an apex angle equal to 90° (half apex angle = 45°), figure 5 presents a comparison between the calculated and the measured normalized amplitude of the pressure field, radiated in the fluid, in a plane perpendicular to the wedge direction. It shows a good agreement between the two curves. The direction of the maximum of amplitude is approximately determined by an angle equal to 67·5° with respect to the antisymmetrical plane.

4. IMMERSED DURALUMIN WEDGE

Duralumin wedges, with different apex angles are studied. In Table 1 their physical constants are given. The same meshes as previously are used and only the material properties are changed in the data files. Figure 6 presents the variations of the wedge wave velocities of the immersed duralumin sample as a function of the apex angle. In this figure, the variations of the wedge wave velocities of the in-air duralumin sample are reproduced and show the effect of the water loading. The agreement is good between the finite element results and the experimental data obtained for the first mode, when the apex angle is smaller than approximately 55°. It is difficult to get experimental results for an apex angle greater than 60° because signals which correspond to the wedge wave and to the Stoneley–Scholte wave are so close that they are mixed. Larger samples would be necessary to get additional data for higher tip angles. Figure 7 presents the variations of the k_z wavenumber, multiplied by the radius R of the external fluid boundary, as a function of the apex angle. This figure is similar to Figure 4, which has been obtained for brass immersed wedges. In the case of duralumin samples, the wedge wave velocity becomes supersonic when the apex angle is greater than approximately 45°. Once again, the theoretical results confirm the existence of propagating and radiating edge modes, because of the complex k_z wavenumber. Figure 8 presents the normalized amplitude of the pressure field in a plane perpendicular to the wedge direction, for a right duralumin sample. Once

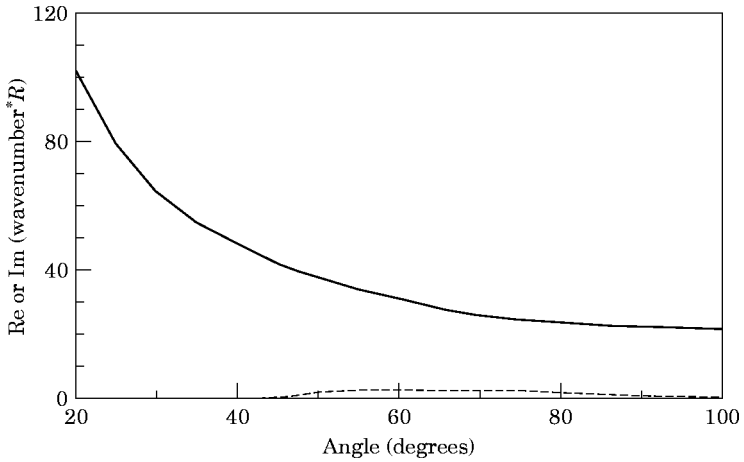

Figure 7. Variations of the k_z wavenumber as a function of the apex angle, for the immersed duralumin wedge. Full line: Re ($k_z R$); dashed line: Im ($k_z R$).

again, the finite element results agree well with the experiments and it shows that the direction of the maximum of amplitude is approximately determined by an angle equal to 65° with respect to the antisymmetrical plane, which is close to the angle for a brass sample. This angle is approximately independent of the wedge angle.

5. COMMENTS ON THE RADIAL COMPONENT OF THE WAVENUMBER

From the finite element calculations, it was evident that in the subsonic regime (i.e., the regime for which the velocity of the wedge wave, V, is smaller than the velocity of propagation in water, V_w), the radial component (k_r) of the wavenumber is imaginary: Im (k_r) is positive which gives rise to an evanescent behaviour of the propagating edge waves in the radial direction. The pressure field is exponentially decaying as a function of the distance to the tip and there is no re-emission in the fluid. This agrees with the fact that the edge wave is confined near the tip of the wedge.

When the wedge wave velocity V is larger than V_w, the calculations exhibit the existence of a propagating radial component, the amplitude of which increases with the distance from the tip of the wedge (Im (k_r) < 0). The study of the origin of this radial increasing is now in progress. A similar anomaly was observed for the generalized Rayleigh wave [18–20]. In fact, a complex angular frequency should be considered instead of a real angular frequency, because of the re-emission in the fluid. Because equation (8) is solved for a given

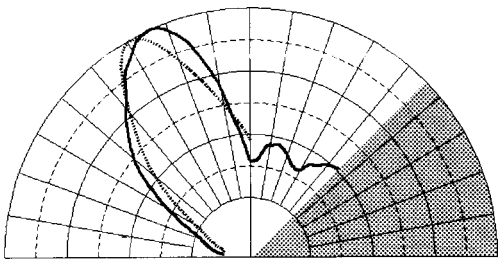

Figure 8. First antisymmetrical wedge mode of a duralumin sample immersed in water. Half apex angle = 45°; $|k_r R| = 35{\cdot}67$. Normalized pressure field in a plane perpendicular to the wedge direction, with a linear scale. Full line: finite element results; dashed line: experimental results.

real angular frequency ω, the imaginary part of relation (4), binding the k_z and the k_r wavenumbers, leads to a negative imaginary part of the radial wavenumber ($\mathrm{Im}\,(k_r) < 0$).

Nevertheless, the method described above gives a precise account of the experimental results, which demonstrates the efficiency of the model.

6. CONCLUSION

In this paper, the propagation of wedge waves along immersed wedges, with the help of the finite element method, has been studied. The formalism has been previously presented [6] but it was restricted to the study of propagating waves along rectilinear wedges. This paper presents a way to solve the finite element system with a view to obtaining both propagating and radiating wedge waves. The agreement between the finite element results and experiments demonstrates the efficiency of the model.

Due to the study of several samples, made of different materials, general trends can be stated, as follows.

When the samples are in air, the limit of the wedge wave velocity for large apex angles (90°) is the Rayleigh wave velocity (V_R).

When the samples are immersed in water, the effect of the water loading induces a decrease in the wedge wave velocity, particularly if the apex angle is small.

If the resulting mode is subsonic, it corresponds to a mode which is propagative in the wedge direction and evanescent in the radial direction, and the displacement of which is located at the tip of the wedge. This mode is found for brass samples, when the apex angle is lower than approximately 60°, and for duralumin samples, when the apex angle is lower than approximately 45°. For Plexiglas samples [6], because the Rayleigh wave velocity is lower than the sound speed in water, wedge waves are subsonic and for a 90° apex angle, it was shown that the wedge wave velocity limit is the Stoneley–Scholte wave velocity [9, 10]. This would be the case for any other material, when the Rayleigh wave velocity is lower than the sound speed in water.

If the resulting mode is supersonic, it is attenuated in the direction of propagation. In that case, for large apex angles, the wedge wave velocities of in-air and in-water samples are close to the Rayleigh wave velocity.

Now, the authors' next aim is to find another way to solve the problem, with a view to considering complex angular frequencies for radiating modes. Then, a further aim is to study the effect of a defect on the wedge or the conversion of modes at the end of the sample [21]. In that case, a transient analysis of the coupled fluid–solid problem has to be performed with the help of the finite element method. Work is now in progress to incorporate this in the ATILA finite element code.

REFERENCES

1. P. E. Lagasse 1973 *Journal of the Acoustical Society of America* **53**, 1116–1122. Higher order finite element analysis of topographic guides supporting elastic surface waves.
2. S. L. Moss, A. A. Maradudin and S. L. Cunningham 1973 *Physical Review B* **8**, 2999–3008. Vibrational edge modes for wedges with arbitrary interior angles.
3. V. V. Krylov 1994 *IEEE Ultrasonics Symposium*, 793–796. Propagation of wedge acoustic waves along wedges imbedded in water.
4. J. R. Chamuel 1993 *IEEE Ultrasonics Symposium*, 313–318. Edge waves along immersed elastic elliptical wedge with range dependent apex angle.
5. A. C. Hladky-Hennion 1996 *Journal of Sound and Vibration* **194**, 119–136. Finite element analysis of the propagation of acoustic waves in waveguides.

6. A. C. Hladky-Hennion, P. Langlet and M. de Billy 1997 *Journal of Sound and Vibration* **200**, 519–530. Finite element analysis of the propagation of acoustic waves along waveguides immersed in water.
7. M. de Billy 1996 *Journal of the Acoustical Society of America* **100**, 659–662. On the influence of loading on the velocity of guided acoustic waves propagating in linear acoustic wedges.
8. S. V. Biryukov, Y. V. Gulyaev, V. V. Krylov and V. P. Plessky 1995 *Surface Acoustic Waves in Inhomogeneous Media*. Berlin: Springer-Verlag.
9. J. G. Scholte 1949 *Proc. Kon. Ned. Akad. Van Wetensch., Amsterdam* **52**, 652–653. On true and pseudo-Rayleigh waves.
10. J. Guilbot 1994 *Thesis Institut National des Sciences Appliquées de Lyon*. Caractérisation acoustique de fonds sédimentaires marins par étude de la dispersion de célérité des ondes d'interface de type Stoneley–Scholte.
11. J. N. Decarpigny 1984 *Thesis Université des Sciences et Techniques de Lille*. Application de la méthode des éléments finis à l'étude de transducteurs piézoélectriques.
12. J. Assaad 1992 *Thesis Université de Valenciennes et du Hainaut-Cambrésis*. Modélisation des transducteurs piézoélectriques haute fréquence à l'aide de la méthode des éléments finis.
13. C. Lanczos 1950 *Journal of Research National Bureau of Standards* **B-45**, 225–280. An iteration method for the solution of the eigenvalue problem of linear differential and integral operators.
14. B. R. Kamal 1986 *Thesis Université des Sciences et Techniques de Lille*, Contribution à l'étude de l'algorithme de Lanczos et applications au calcul dynamique de structures.
15. C. Rajakumar and C. R. Rogers 1991 *International Journal of Numerical Methods for Engineering* **32**, 1009–1026. The Lanczos algorithm applied to unsymmetric generalized eigenvalue problem.
16. P. E. Lagasse, I. M. Mason and E. A. Ash 1973 *IEEE Transactions on Microwave Theory and Techniques* **MTT-21**, 225–236. Acoustic surface waveguides—analysis and assessment.
17. M. de Billy 1996 *Ultrasonics* **34**, 611–619. Acoustic technique applied to the measurement of the free edge wave velocity.
18. L. M. Brekhovskikh 1960 *Waves in layered media*. New York: Academic Press.
19. H. Uberall 1973 *Physical Acoustics* **9**, 1–60. Surface waves in acoustics.
20. G. Quentin, A. Derem and B. Poiree 1990 *Journal d'Acoustique* **3**, 321–336. The formalism of evanescent plane waves and its importance in the study of the generalized Rayleigh wave.
21. M. de Billy 1997 *Journal of the Acoustical Society of America* **101**, 3261–3269. On the scattering of antisymmetric edge modes.